Available online at www.sciencedirect.com
SCIENCE DIRECT
Polymer 46 (2005) 12322–12336
polymer
www.elsevier.com/locate/polymer

# Co-continuous and encapsulated three phase morphologies in uncompatibilized and reactively compatibilized polyamide 6/polypropylene/polystyrene ternary blends using two reactive precursors

T.S. Omonov, C. Harrats *, G. Groeninckx

*Laboratory of Macromolecular Structural Chemistry, Division of Molecular and Nanomaterials, Department of Chemistry, Katholieke Universiteit Leuven, Celestijnenlaan 200 F, 3001 Heverlee-Leuven, Belgium*

Received 21 February 2005; received in revised form 1 August 2005; accepted 4 October 2005
Available online 3 November 2005

**Abstract**

Phase morphology development in ternary uncompatibilized and reactively compatibilized blends based on polyamide 6 (PA6), polypropylene (PP) and polystyrene (PS) has been investigated. Reactive compatibilization of the blends has been performed using two reactive precursors; maleic anhydride grafted polypropylene (PP-*g*-MA) and styrene maleic anhydride copolymer (SMA) for PA6/PP and PA6/PS pairs, respectively. For comparison purposes, uncompatibilized and reactively compatibilized PA6/PP and PA6/PS binary blends, were first investigated. All the blends were melt-blended using a co-rotating twin-screw extruder. The phase morphology investigated using scanning electron microscope (SEM) and selective solvent extraction tests revealed that PA6/PP/PS blends having a weight percent composition of 70/15/15 is constituted from polyamide 6 matrix in which are dispersed composite droplets of PP core encapsulated by PS phase. Whereas, a co-continuous three-phase morphology was formed in the blends having a composition of 40/30/30. This morphology has been significantly affected by the reactive compatibilization. In the compatibilized PA6/(PP/PP–MA)/(PS/SMA) blends, PA6 phase was no more continuous but gets finely dispersed in the PS continuous phase. The DSC measurements confirmed the dispersed character of the PA6 phase. Indeed, in the compatibilized PA6/(PP/PP–MA)/(PS/SMA) blends where the PA6 particle size was smaller than 1 μm, the bulk crystallization temperature of PA6 (188 °C) was completely suppressed and a new crystallization peak emerges at a lower temperature of 93 °C as a result of homogeneous nucleation of PA6.


*Keywords:* Ternary polymer blends; Polyamide 6; Polypropylene

## 1. Introduction

In spite of the huge number of studies devoted to the compatibilization of binary polymer blends, only few deal with blends containing three or more components [1–13]. To avoid confusion with the vocabulary used in literature to identify 'ternary blends', in this report a 'ternary blend' is constituted of three different immiscible components, which are non-reactive towards each other. Many ternary blends considered in literature contain at least two miscible phases and/or one of the components is a compatibilizer. Typical examples are acrylonitrile–butadiene–styrene/poly(phenylene ether)/polystyrene (ABS/PPE/PS) [1], PPE/PS/SAN (styrene–acrylonitrile) [2], polycarbonate/polyvinylidienefluoride/polymethylmethacrylate [4]. Compatibilization of the first two blends is similar to classical binary blends as PPE is miscible with PS at all proportions. The styrene phase of the ABS or that of the SAN copolymer ensures compatibilization with the (PPE/PS) phase provided that the acrylonitrile content is appropriately adjusted.

Polyolefin based blends including low-density polyethylene (LDPE), linear low-density polyethylene (LLDPE), high-density polyethylene (HDPE) and polypropylene (PP) are among the components of multicomponent blends reported in literature [10]. A ternary blend containing LDPE, HDPE and PP immiscible components has been reactively compatibilized using liquid polybutadiene (PB), maleated or not, and a dialkyl peroxide as a free radical initiator. Liquid PB without functional groups was an effective compatibilizer for the virgin polyolefins, while maleated PB was necessary for the blends prepared from recycled polyolefin. In this case, the reactively generated copolymers, which ensured compatibilization were not identified and their structures were poorly controlled. The control of the process of free radical chain attack is not possible under melt-compounding operation.

* Corresponding author. Tel.: +32 16 327441.
*E-mail address:* charef.harrats@chem.kuleuven.be (C. Harrats).

0032-3861/$ - see front matter © 2005 Elsevier Ltd. All rights reserved.
doi:10.1016/j.polymer.2005.10.022

Ha et al. studied the effect of a pair of compatibilizers including chlorinated polyethylene (CPE) and ethylene–propylene rubber (EPR) on the ternary blends of HDPE, PP and poly(vinyl chloride) HDPE/PP/PVC at a fixed composition of (80/10/10) [12]. The resulting phase morphology was not clearly described, but a significant improvement in impact strength of the compatibilized blends was claimed. A quaternary blend composed of immiscible LDPE/PVC/PP/PS in the ratio of 70/10/10/10 was compatibilized using a mixture of chlorinated polyethylene (CPE), ethylene–propylene–diene monomer (EPDM) and styrene–butadiene–styrene (SBS) copolymer. The accent was put on the investigation of the ultimate mechanical properties of the blends including the impact strength, the tensile strength to break and the elongation to break. The compatibilized blends showed a significant improvement in the mechanical properties when peroxide was added to the compatibilizing mixture. Unfortunately, the authors did not provide a clear view on the phase morphology developed when the four immiscible polymers are melt-mixed together in the presence of a ternary compatibilizing mixture.

One of the challenges met in considering ternary blends is the investigation and understanding of the phase morphology developed [14–19]. A composite (droplet-in-droplet) phase morphology was formed when a ternary immiscible blend containing HDPE, PS and PMMA was melt-mixed so that the HDPE phase constitutes the matrix and the PS and the PMMA components the dispersed phases [14]. The effect of the molecular weight of each of the PS or the PMMA on droplet encapsulation was investigated. It was shown that depending on the molecular weight of the PS and PMMA, PS could be made to encapsulate PMMA and PMMA could also be made to encapsulate PS.

Hobbs et al. used Harkin's spreading coefficient concept [20] to interpret their observations on the phase morphology of different ternary blends. The use of this coefficient allowed a correct prediction of the phase morphologies developed in the system of multicomponent blends considered by the authors [17].

Guo et al. have modified these concepts by the introduction of both the interfacial tensions and the interfacial areas of the blend to predict the phase structures of different ternary [18] and quaternary [19] polymer blends of polyethylene (PE), polypropylene (PP), polystyrene (PS) and poly(methy1 methacrylate) (PMMA). The phase morphology of a PP/HDPE/PS (70/20/10) blend having a separation-type phase morphology (HDPE + PS) has changed by the addition of 1 wt% poly(styrene-*b*-ethylene) (S–E) block copolymer to an encapsulation-type (PS encapsulated by HDPE). The encapsulation of the PS by PE was more complete when 3% S–E block copolymer is added to this system. When HDPE was the matrix in the 70/20/10 HDPE/PP/PS ternary blend, PS particles were encapsulated by PP phase [18]. By addition of 2 wt% of the S–E block copolymer PS and PP phases were dispersed separately in the HDPE matrix. In this work, the theoretical predictions were in a good agreement with the experimental results.

In the present study, two ternary blends were investigated including 70/15/15 and 40/30/30 PA6/PS/PP. Reactive compatibilization was ensured using two reactive precursors; maleic anhydride grafted polypropylene (PP–MA) for PA/PP and styrene-*co*-maleic anhydride (SMA) for PA/PS pair. Note that polyamide is reactive towards these two precursors via its amine end groups. Numerous studies have reported on the compatibilization of polyamides using maleated polymers [21–28]. The efficiency of compatibilization which results from the generation in situ of the graft copolymer was proved by the observed particle size reduction of the minor phase [29–31].

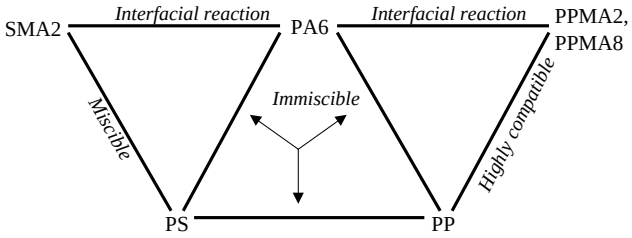


Fig. 1. Schematic representation of the strategy of compatibilization used for PA6/PP/PS ternary blends.

The aim of this study is to understand and identify the phase morphology developed in a blend having three immiscible components when appropriate compatibilizers are in situ generated during the melt-blending operation. The ultimate objective is to state with respect to the components 'which is which' when the phase morphology is characterized. In Fig. 1 is illustrated a scheme showing the components considered in the design of the ternary blends and the compatibilizing system used for their reactive compatibilization.

## 2. Experimental

### 2.1. Materials

The polyamide 6 used is Akulon K134 supplied by DSM Research; ($M_n$ = 35,000, $T_m$ = 221 °C, $T_c$ = 188 °C, a melt-viscosity of 296 Pa s (260 °C, 100 rad/s). The polypropylene is a Borealis grade having the following characteristics: MFI = 12 g/10 min, $T_m$ = 163 °C and $T_c$ = 122 °C, a melt-viscosity of 229 Pa s (260 °C and 100 rad/s). The polystyrene is Styron 660-7 grade from DOW Chemical having a MFI = 7 g/10 min, $T_g$ = 109 °C, a melt-viscosity of 149 Pa s (260 °C, 100 rad/s). Two grades of maleic anhydride grafted polypropylene PP–MA2 and PP–MA8 having 2 and 8 wt% maleic anhydride group, respectively, have been used as reactive precursors for the compatibilization of PA6 and PP blends. PP-MA2 is Exxelor PO 1020 from Exxon Mobile, and PP-MA8 is Epolene E43 from Eastman Kodak. Styrene maleic anhydride copolymer SMA2 containing 2 wt% of maleic anhydride was supplied by Bayer. The PP-MA precursors were purified from ungrafted residue of MA monomer by dissolution in hot toluene and successive precipitation in acetone.

### 2.2. Blends preparation

The blends were prepared using a twin-screw mini-extruder (DSM-Research, The Netherlands). It consists of a mixing chamber with a capacity of 15 ml and two co-rotating conical

Table 1
Binary and ternary blends prepared

| Blends | Composition (wt%) |
|---|---|
| Uncompatibilized | |
| PA6/PS | 85/15; 70/30 |
| PA6/PP | 85/15; 70/30 |
| PA6/PP/PS | 70/15/15; 40/30/30 |
| Compatibilized | |
| PA6/(PS/SMA2) | 85/(12.5/2.5); 70/(25/5) |
| PA6/(PP/PP–MA2) | 85/(12.5/2.5); 70/(25/5) |
| PA6/(PP/PP–MA8) | 85/(12.5/2.5); 70/(25/5) |
| PA6/(PP/PP–MA2)/(PS/SMA2) | 70/(12.5/2.5)/(12.5/2.5); 40/(25/5)/(25/5) |
| PA6/(PP/PP–MA8)/(PS/SMA2) | 70/(12.5/2.5)/(12.5/2.5); 40/(25/5)/(25/5) |

screws. By means of a re-circulation channel within the mixing chamber and a valve to open the mixing chamber, the residence time can be varied. The mixing chamber can be saturated with nitrogen gas during melt blending to avoid oxidative degradation of the components. The extrusion temperature was kept constant at 260 °C, the screw speed was fixed at 100 rpm after all the ingredients were fed into the barrel. The blending was carried out for 10 min. Prior to blending PA6 was vacuum dried. The mixing time is recorded from the moment all the dry-premixed components were fed into the extruder. The series of blends prepared are listed in Table 1.

### 2.3. Phase morphology characterization

Two types of surfaces, a cryofractured and cryosmoothed where a phase or two were etched using a selective solvent, were observed using scanning electron microscopy. The cryosmoothing was performed at a temperature of −100 °C using a ultramicrotome (Leica Ultracut UCT) equipped with a glass knife.

Knowing that co-continuity index of blend components depends on the thickness of the blend extracted [32] the samples for the selective extraction have been prepared from the strands of the blends with the thickness of 2–3 mm and with the weight of 20–40 mg.

To determine the blend components co-continuity, samples of known weight were stirred in a selective solvent 7 days to extract the respective phase. Formic acid used to etch the PA6 phase (at 50 °C), xylene for the PP phase (at 90 °C) and chloroform for PS phase (at 50 °C). After extraction procedure the samples were dried in the vacuum oven at a temperature of 80 °C for a one day and the mass of the samples was determined. The phase co-continuity is quantified based on the ratio of the extracted fraction to the initially present fraction of the same species using the expression:

$$\%\ \text{cocontinuity } 'X'\ \text{phase} = \frac{\text{Sample weight} - \text{weight after extraction of } 'X'\ \text{phase}}{\text{weight of } 'X'\ \text{phase before extraction}} \times 100\%$$

where '*X*' is PA6, PP or PS phase.

After etching and drying procedure, the samples were coated with gold using Balzers sputtering device. The obtained digital SEM micrographs of the cryosmoothed surfaces were analyzed for the determination of number average diameter of the dispersed particles using a Leica QWin image analysis software. An average of 300–500 particles were collected from several micrographs. The characteristic number average particle diameters ($\bar{D}_n$) are given where the composition had a matrix/droplet morphology and the average sizes were not corrected for the fact that not all droplets were cut at their largest cross-section.

### 2.4. Differential scanning calorimetry (DSC)

DSC measurements were performed using DSC Pyris 1 series (Perkin Elmer). The temperature and heat flow calibrations were performed using indium ($T_m$ = 156.6 °C) and tin ($T_m$ = 231.88 °C) at a heating and a cooling rate of ± 10 °C/min. Empty pan measurements were performed at the beginning of each series of tests. The sample was heated at a heating rate of 40 °C to a temperature of 260 °C where it is kept for 5 min to remove thermal history. Then, the sample was cooled down at −10 °C/min to 0 °C. Subsequent melting scans were recorded at a heating rate of 10 °C/min. In all the cases the sample weight was about 6 mg.

### 2.5. Rheological measurements

The dynamic viscosity of the raw materials was measured using a DSR dynamic rheometer of Rheometrics. Molded discs from the various materials of 1 mm thick and 25 mm of diameter were used. The viscosity was measured at a temperature of 260 °C and a frequency sweep from 100 to 1 rad/s. Prior to testing, the samples were checked for their linear viscoelastic behavior by carrying out a strain sweep test at a fixed frequency of 1 rad/s.

## 3. Results and discussion

### 3.1. PA6/PP and PA6/PS binary blends

Prior to the study of the ternary PA6/PP/PS blends a complete view on the phase morphology development and compatibilization of the individual uncompatibilized and compatibilized PA6/PP and PA6/PS binary blends is necessary. Figs. 2 and 3 show the SEM micrographs of the non-compatibilized binary PA6/PS and PA6/PP blends. As expected, both polystyrene and polypropylene are immiscible with polyamide 6 [18]. The interfacial adhesion between PS particles and PA6 matrix in PA6/PS blend (Fig. 2(a) and (a′))or PP particles and PA6 matrix in the PA6/PP blend (Fig. 3(a) and (a′)) is very poor. Indeed, all the particles debonded from the matrix are clearly loose on the cryofractured surfaces. The surfaces of the particles are smooth without any visible roughness (the surface roughness of particles is usually expected in case of good interfacial adhesion between the particles and the matrix).

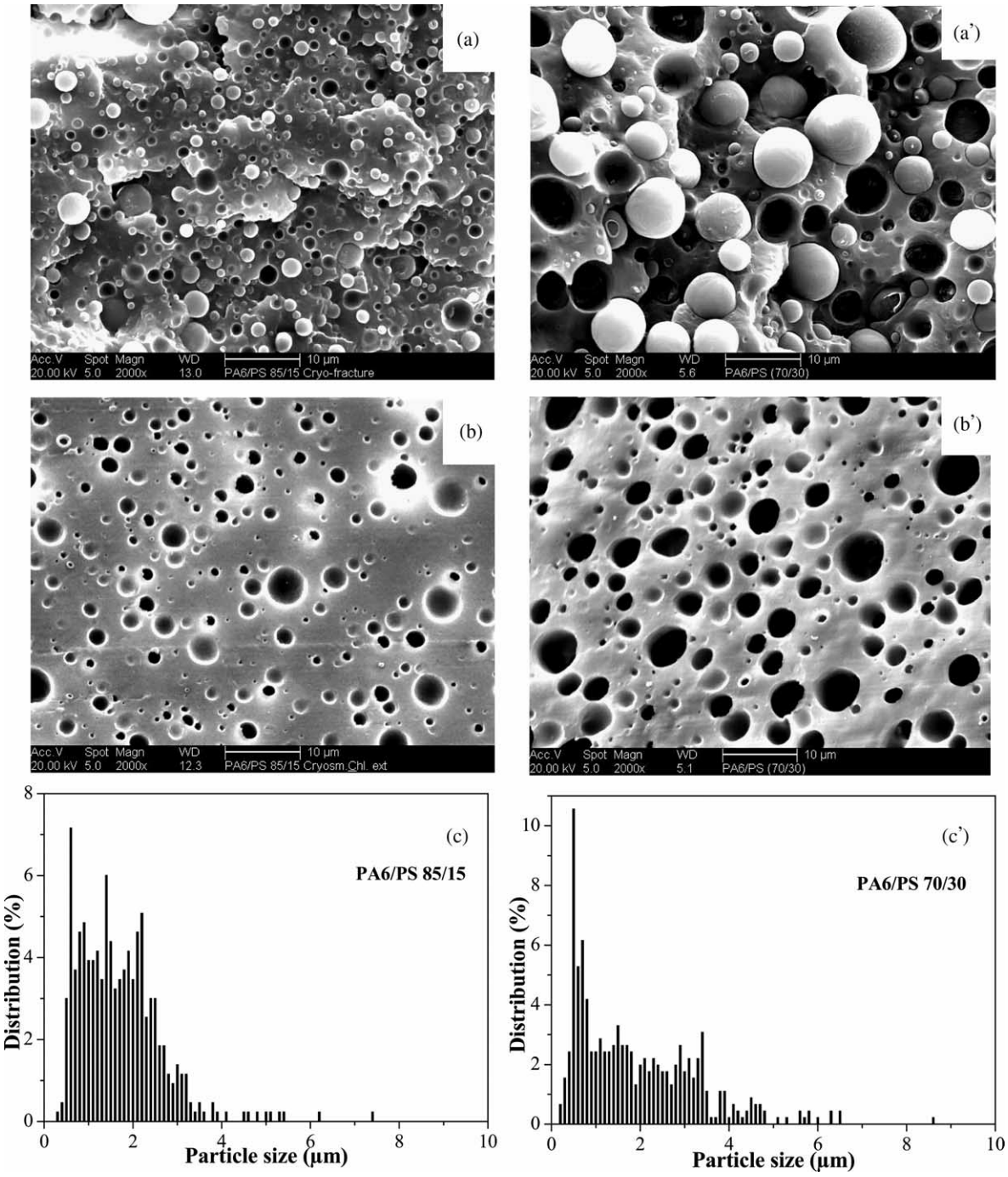


Fig. 2. Morphology of the 85PA6/15PS (a, b) and 70PA6/30PS (a′, b′) blends: (a, a′) cryofractured surface, (b, b′) cryosmoothed and PS phase extracted using chloroform, (c, c′) particle size distribution.

As shown in Table 2, average particle sizes of 1.8 and 2 μm are obtained in the absence of compatibilizer in 85PA6/15PS and 70PA6/30PS blends, respectively. This particle size increase upon the increase of the minor phase content is expected since the process of particle–particle coalescence is favored by increasing the minor phase concentration. Similarly, the particle size distribution of PS phase gets broader when the minor phase concentration is increased (compare histograms c and c′ in Fig. 2). Fig. 3 illustrates the phase morphology of 85PA6/15PP and 70PA6/30PP uncompatibilized blends. The former blend exhibits an average particle size of 2.3 μm. Whereas, as expected, coarser PP particles having an average diameter of 3.2 μm are obtained in the latter blend. For the same reasons of favored coalescence, a broader particle size distribution is observed in the blends containing 30 wt% PP compared to blends containing only 15 wt% (compare histograms c and c′ of Fig. 3).

Note that the average particle size in PA6/PS is smaller than that in PA6/PP blend at both compositions investigated (Table 2). This picture of particle size difference does not

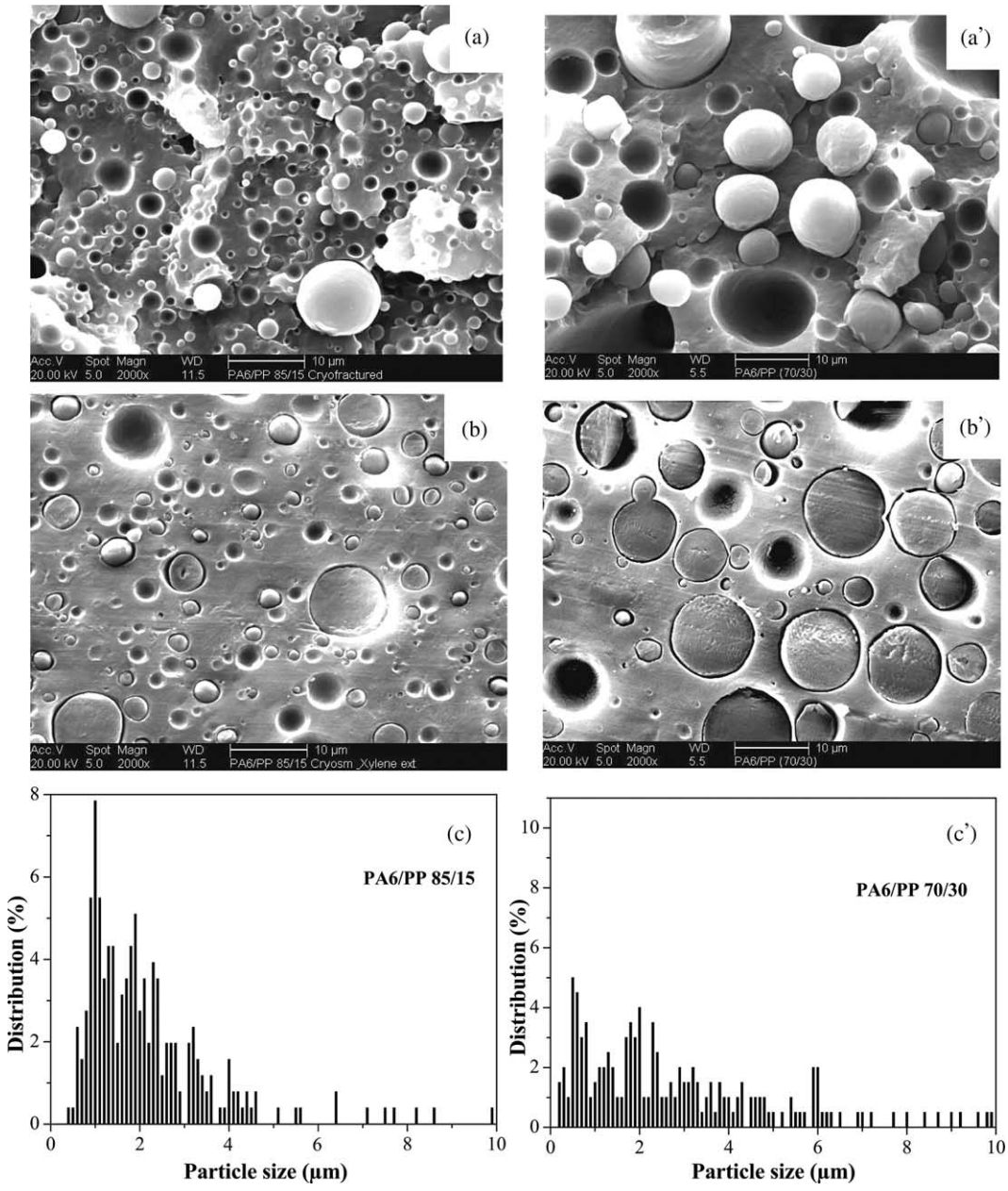


Fig. 3. Morphology of the 85PA6/15PP (a, b) and 70PA6/30PP (a′, b′) blends: (a, a′) cryofractured surface, (b, b′) cryosmoothed surfaces and (c, c′) particle size distribution.

translate the equality in the interfacial tensions between the two pairs (Table 3: $\sigma_{PA6/PP} \cong \sigma_{PA6/PS}$), but is rather due to the significant difference in the viscosity ratio between the two pairs.

The shear rate generated in the mini twin-screw extruder using a screw rotation speed of 100 rpm has been approximated to 100 $s^{-1}$ [33,34]. Hence, the ratios are calculated from the dynamic data at 100 rad/s.

As shown in Fig. 4 polypropylene is more viscous than polystyrene by factor of 1.52.

As a compatibilizer precursor for the PA6/PS blends styrene maleic anhydride was used which is miscible with PS over the whole composition range [35]. As illustrated in Table 2 or Fig. 5, the addition of 2.5 wt% of the reactive precursor SMA2

Table 2
The value of number average particle size ($\bar{D}_n$) for the uncompatibilized and compatibilized binary blends

| Uncompatibilized blends | $\bar{D}_n$ (μm) | |
|---|---|---|
| | Composition 85/15 | Composition 70/30 |
| PA6/PS | 1.8 | 2.0 |
| PA6/PP | 2.3 | 3.2 |
| Compatibilized blends | $\bar{D}_n$, (μm) | |
| | Composition 85/(12.5/2.5) | Composition 70/(25/5) |
| PA6/(PS/SMA2) | 0.6 | 0.4 |
| PA6/(PP/PPMA2) | 2.0 | 3.0 |
| PA6/(PP/PPMA8) | 0.8 | 0.8 |

Table 3
Calculated values and literature data of the interfacial tensions between PA6, PP and PS homopolymers

| Interfacial tension (mN/m) | Calculated | Literature data | | | | |
|---|---|---|---|---|---|---|
| $\sigma_{PA6/PP}$ | 13.64 | 13.3 [42] (250 °C) | 13.61 [40] (230 °C) | 7.8 [42] (250 °C) | 15.4–16.3 [47] (260 °C) | 12.4 [48] (225 °C) |
| $\sigma_{PA6/PS}$ | 13.72 | 20.0 [45] (230 °C) | 7.3 [46] (240 °C) | 10 [49] (230 °C) | 7.63 [44] (230 °C) | |
| $\sigma_{PP/PS}$ | 2.26 | 2.0 [43] (260 °C) | 4.8 [41] (200 °C) | 6.46 [50] (200 °C) | 6.25 [51] (200 °C) | 4.3 [41] (230 °C) |

containing 2 wt% of maleic anhydride to the PA6/PS binary blend reduced significantly the average dimension of the PS dispersed phase at both blend compositions. The sizes of the PS particles are reduced by factors of 3 and 5 in 85/15 and 70/30 compatibilized blends, respectively. The particle size distribution gets narrower than that in uncompatibilized blends. That is a clear indication of the in situ generation of the grafted PA6-*g*-PS copolymer during melt-blending as a result of the amine–maleic anhydride imidation reaction [21,29,36].

In contrast, the PP-MA2 which also contains 2 wt% of maleic anhydride groups does not produce comparable (as SMA2 in PA6/PS) extent of size reduction of the PP particles in PA6/PP compatibilized blend (Fig. 6). Only a slight phase size decrease is recorded in the 85/15 blend (2 μm compared to 2.3 μm in uncompatibilized blend). In fact, at equivalent maleic anhydride content and total amount of precursor, SMA2 produces dispersed particles that are much smaller in the PA6/PS blend than those formed from PP-MA2 compatibilizer precursor in the PA6/PP blend. Probably SMA2 copolymer might easily diffuse and reacts at the interface with the PA6 than does PP–MA2. When the MA content was increased to 8 wt% (PP–MA8) the compatibilizing effect is tremendous compared to PP–MA2, but still remains less efficient than SMA2 in PA6/PS (Table 2, Fig. 7). Note that the particle size distribution induced by PP–MA8 exhibits a bimodal pattern due to the formation of larger and non-spherical particles as visible in the SEM picture of Fig. 7(b′).

### 3.2. PA6/PP/PS ternary blends

Two blend compositions were considered including a 70PA6/15PS/15PP where droplets of PP and PS are expected in a PA6 matrix, and a 40PA6/30PS/30PP where phase co-continuity was aimed at.

#### 3.2.1. 70PA6/15PP/15PS blends

An example of the morphologies resulting from the melt-compounding of uncompatibilized 70PA6/15PP/15PS is shown in Fig. 8. The cryofractured surface shown in Fig. 8(a) reveals the existence of encapsulated droplets dispersed in PA6 matrix. The shells surrounding the core particles are broken upon the cryofracturing of the sample. From this picture one is not able to indicate which phase is where? In Fig. 8(b) is presented a SEM picture of a cryosmoothed surface of the same blend where polystyrene phase was removed using chloroform. This test evidences that polystyrene constitutes the shell of the encapsulated structures and the core is the polypropylene phase. The average shell thickness is less than 1 μm but larger than 0.2 μm. A close observation of the SEM micrograph reveals that isolated polystyrene particles (see white circles) as well as partly encapsulated polypropylene particles (see dashed circles) were also formed during the blend compounding.

According to Hobbs et al. [17] it is possible to predict qualitatively the type of the phase morphology developed in a ternary immiscible polymer blend by using the concept of the spreading coefficient as initially introduced by Harkin [20]. Indeed for our case the ternary blend has PA6 as a matrix and two dispersed phases; PP and PS. The spreading coefficient $\lambda_{PP/PS}$ of PP phase on PS phase is:

$$\lambda_{PP/PS} = \sigma_{PA6/PS} - \sigma_{PA6/PP} - \sigma_{PP/PS} \quad (1)$$

where $\sigma_{ij}$ is the interfacial tension between $i$ and $j$ components.

If $\lambda_{PP/PS}$ is positive, then PP phase will encapsulate PS phase. Similarly, if $\lambda_{PS/PP}$ (Eq. (2)) is positive then PS phase will encapsulate PP phase.

$$\lambda_{PS/PP} = \sigma_{PA6/PP} - \sigma_{PA6/PS} - \sigma_{PS/PP} \quad (2)$$

If both $\lambda_{PP/PS}$ and $\lambda_{PS/PP}$ are negative, the PP and the PS phases will remain separately dispersed (isolated) in PA6 matrix. Although this concept was successful to predict the phase morphologies claimed [17–19], it fails in our case because the development of the phase morphologies in polymer melt depends also on other key factors such as the viscosity and elasticity of the blend. The use of the interfacial tension alone

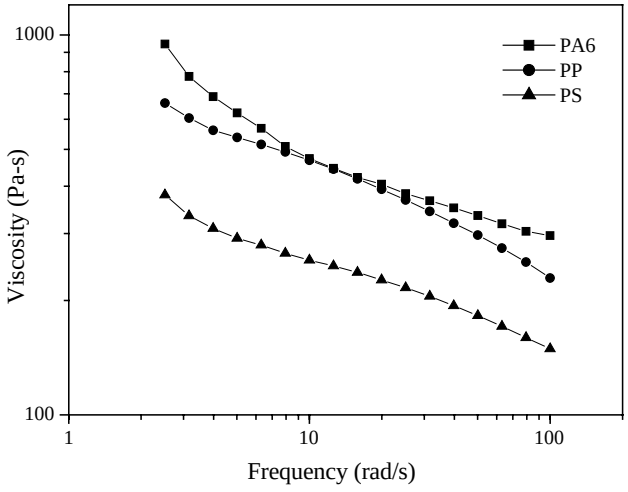


Fig. 4. Viscosity vs. frequency for the pure polymers at 260 °C.

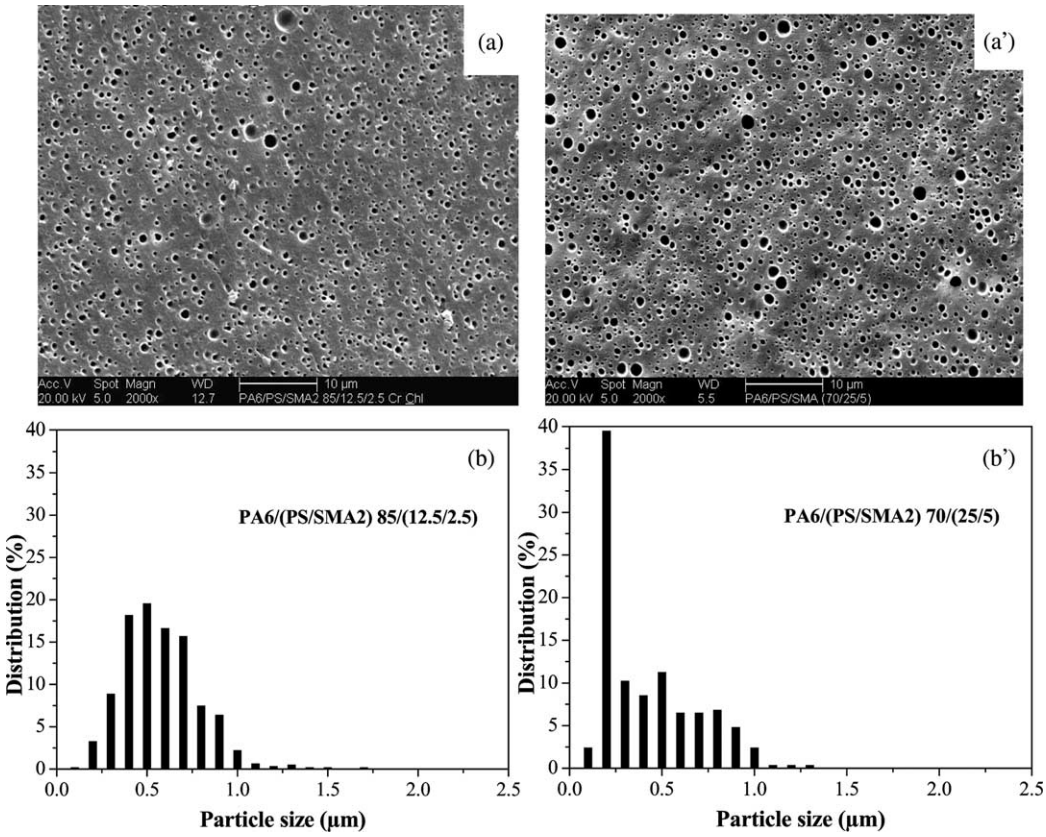


Fig. 5. Morphology of PS phase extracted surfaces using chloroform of: (a) 85PA6/(12.5/2.5)(PS/SMA2), (b) 70PA6/(25/5)(PS/SMA2) blends, (b, b′) particle size distribution.

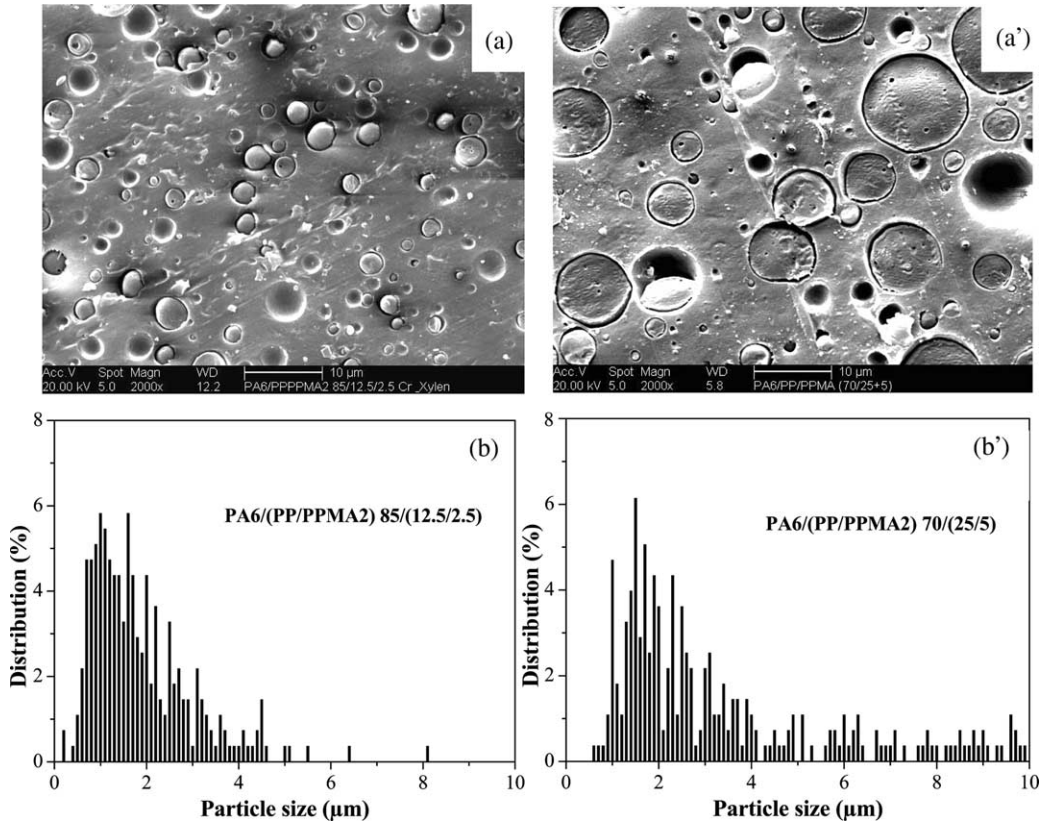


Fig. 6. Morphology of cryo-smoothed surfaces of: (a) 85PA6/(12.5/2.5)(PP/PP–MA2), (b) 70PA6/(25/5)(PP/PP–MA2) blends, (b, b′) particle size distribution.

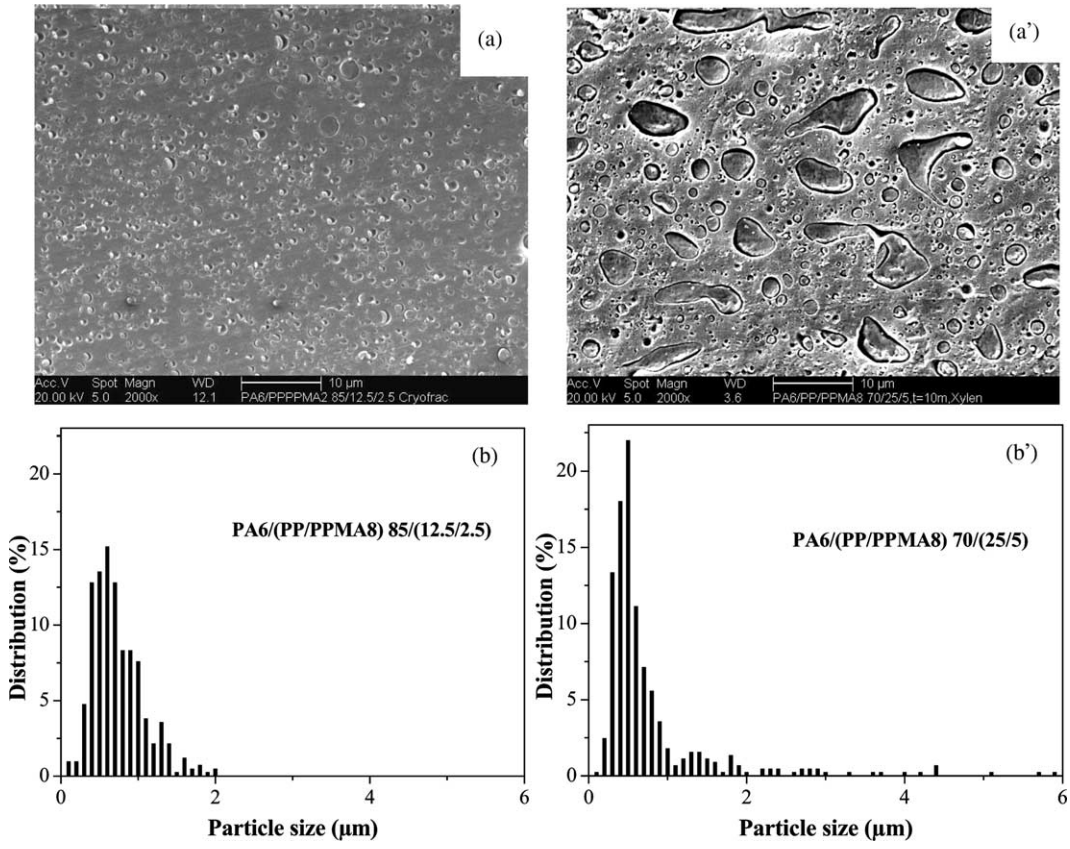


Fig. 7. Morphology of cryosmoothed surfaces of: (a) 85PA6/(12.5/2.5)(PP/PP–MA8), (b) 70PA6/(25/5)(PP/PP–MA8) blends, (b, b′) particle size distribution.

for the prediction of the type of phase morphologies in immiscible polymer melt can be successful in blend components having closer melt viscosities. The application of these equations using values of the interfacial tensions calculated based on the surface tension data by using harmonic mean equation [37], or obtained from literature [37–49] (Table 3) for each pairs of components, was not able to predict the type of phase morphology observed in our present system.

The interfacial tension were calculated for the three polymer–polymer interface present in the blends, i.e. PA6/PP, PA6/PS and PP/PS using expression:

$$\sigma_{12} = \sigma_1 + \sigma_2 - \frac{4\sigma_1^{\mathrm{d}}\sigma_2^{\mathrm{d}}}{\sigma_1^{\mathrm{d}} + \sigma_2^{\mathrm{d}}} - \frac{4\sigma_1^{\mathrm{p}}\sigma_2^{\mathrm{p}}}{\sigma_1^{\mathrm{p}} + \sigma_2^{\mathrm{p}}} \tag{3}$$

where $\sigma_{ij}$ is the interfacial tension between the components $i$ and $j$. $\sigma_i$ is the surface tension of component $i$, $\sigma_i^{\mathrm{d}}$ is the dispersive fraction of the surface tension of component $i$ and $\sigma_i^{\mathrm{p}}$ is the polar fraction of the surface tension of component $i$.

In this work, interfacial tension values between the two blend components were estimated from the surface tension values and polarities obtained from literature data [37–39] and extrapolated to the compounding temperature of the components (260 °C) using the values of $\mathrm{d}\sigma_i/\mathrm{d}T$. Extrapolation of the surface tensions values for blend components has been carried out using:

$$\sigma_i = \frac{\partial \sigma_i}{\partial T} T + K_i \tag{4}$$

From the values obtained and assuming that $\sigma_i = \sigma_i^{\mathrm{p}} + \sigma_i^{\mathrm{d}}$, we can derivate the data for calculating of interfacial tension at 260 °C, which is highlighted below:

| Polymer | $\sigma_i$ (mN/M) | $\sigma_i^{\mathrm{p}}$ (mN/m) | $\sigma_i^{\mathrm{d}}$ (mN/m) | $\mathrm{d}\sigma_i/\mathrm{d}T$ (mN/m/°C) |
|---|---|---|---|---|
| PA6 | 36.42 | 13.2 | 23.22 | −0.065 |
| PP | 15.94 | 0.37 | 15.57 | −0.056 |
| PS | 23.44 | 0.168 | 22.272 | −0.072 |

In fact, in all cases the spreading coefficient was negative which means that PP and PS should be separately dispersed in the PA6 matrix. That was the opposite of the observed phase morphologies in which polystyrene was encapsulating the polypropylene phase (Fig. 8).

As known the equilibrium phase structure of a multiphase system is determined not by interfacial tension alone, but rather by the interfacial free energy which represents combination of interfacial tension and interfacial areas [18]. Guo et al. have modified Hobbs phase concepts to include both interfacial tension and interfacial areas, and have successfully used the resulting expressions to predict phase morphologies in a ternary [18] and quaternary [19] systems. Based on the modified phase concept the phase morphology of the multicomponent blend system will be that which has the lowest free energy.

The interfacial free energies of the PA6/PP/PS ternary blend (where PA6 is a matrix phase) for different phase structures can

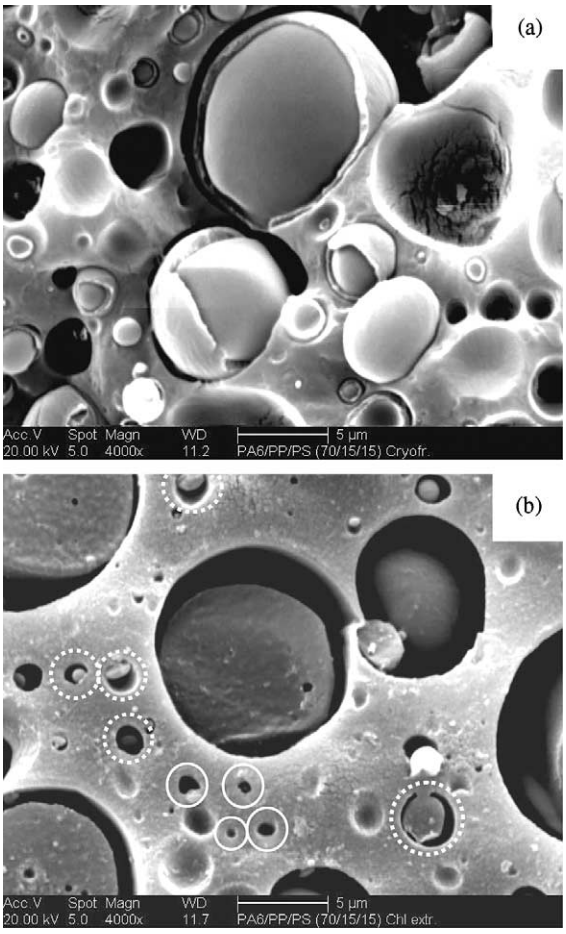


Fig. 8. Morphology of the ternary 70PA6/15PP/15PS blends: (a) cryofractured, (b) chloroform extracted surfaces.

also be calculated by using the following equations:

$$\left(\sum A_i\gamma_{ij}\right)_{\mathrm{PP+PS}} = (4\pi)^{1/3}\left[n_{\mathrm{PP}}^{1/3}\left(\frac{V_{\mathrm{PP}}}{V_{\mathrm{PS}}}\right)^{2/3}\gamma_{\mathrm{PA6/PP}} + n_{\mathrm{PP}}^{1/3}\gamma_{\mathrm{PA6/PS}}\right](3V_{\mathrm{PS}})^{2/3}$$

$$\left(\sum A_i\gamma_{ij}\right)_{\mathrm{PP/PS}} = (4\pi)^{1/3}\left[n_{\mathrm{PP}}^{1/3}\left(1+\frac{V_{\mathrm{PP}}}{V_{\mathrm{PS}}}\right)^{2/3}\gamma_{\mathrm{PA6/PP}} + n_{\mathrm{PS}}^{1/3}\gamma_{\mathrm{PP/PS}}\right](3V_{\mathrm{PS}})^{2/3} \quad (5)$$

$$\left(\sum A_i\gamma_{ij}\right)_{\mathrm{PS/PP}} = (4\pi)^{1/3}\left[n_{\mathrm{PP}}^{1/3}\left(\frac{V_{\mathrm{PP}}}{V_{\mathrm{PS}}}\right)^{2/3}\gamma_{\mathrm{PP/PS}} + n_{\mathrm{PS}}^{1/3}\left(1+\frac{V_{\mathrm{PP}}}{V_{\mathrm{PS}}}\right)^{2/3}\gamma_{\mathrm{PA6/PS}}\right](3V_{\mathrm{PS}})^{2/3}$$

where $n_{\mathrm{PP}}$ and $n_{\mathrm{PS}}$ are number of the particles of PP and PS phases in the system, $\gamma_{ij}$ is the interfacial tension values between $i$ and $j$ components, $V_{\mathrm{PP}}/V_{\mathrm{PS}}$ is the volume ratio of PP and PS phases.

For the simplicity we have assumed that the number of the PP and PS particles is the same, i.e. $n_{\mathrm{PP}}=n_{\mathrm{PS}}=n$ and volume ratio of the phases is unit, i.e. $V_{\mathrm{PP}}=V_{\mathrm{PS}}=V$. Interfacial tension values used were taken from the Table 3.

Using these assumptions we can rewrite above mentioned equations for the three possible phase structures where PA6 is a matrix phase:

$$\left(\sum A_i\gamma_{ij}\right)_{\mathrm{PP+PS}} = (36\pi nV^2)^{1/3}(\gamma_{\mathrm{PA6/PP}}+\gamma_{\mathrm{PA6/PS}})$$

$$\left(\sum A_i\gamma_{ij}\right)_{\mathrm{PP/PS}} = (36\pi nV^2)^{1/3}(2^{2/3}\gamma_{\mathrm{PA6/PP}}+\gamma_{\mathrm{PP/PS}}) \quad (6)$$

$$\left(\sum A_i\gamma_{ij}\right)_{\mathrm{PS/PP}} = (36\pi nV^2)^{1/3}\left(\gamma_{\mathrm{PP/PS}}+2^{2/3}\gamma_{\mathrm{PA6/PS}}\right)$$

Now, it is clear that the value of interfacial free energies depends on interfacial tension values. In that case the structure of PP+PS in a PA6 matrix has a highest value. The lowest interfacial free energy value belongs to a structure of PP/PS. Therefore, we would predict that the PS phase will be encapsulated by the PP phase in such blends. But, again, in our blends experimentally observed phase morphologies are not in agreement with the theoretically predicted ones.

Note, as mentioned before we have assumed in our predictions that the number of PP and PS particles is the same, which may not be true in a real blend case. Although, Guo et al. noted that the calculations based on a actual particle sizes gives essentially the same results based on the assumption of equal number of particles [17].

Addition of 2.5 wt% of each of SMA2 and PP–MA reactive precursors for the compatibilization of PA6/PS and PA6/PP, respectively, modified significantly the developed phase morphology. The SEM micrographs of cryofractured surfaces of 70PA6/(12.5/2.5)(PP/PP–MA2)/(12.5/2.5)(PS/SMA2) blend is presented in Fig. 9(a). The selective etching of the polystyrene phase from the cryosmoothed surfaces using chloroform shows the remaining PP phase in PA6 matrix (Fig. 9(b)). This picture reveals a mixed situation of phase morphology, i.e. a part of PP particles are encapsulated by the PS phase and a large number of isolated PS particles are visible as dark holes. Note also that the encapsulated PP particles exhibit a broad particle size distribution. A rough volume estimation, shows that about 70% of the polystyrene phase forms its own domains as isolated particles dispersed in the PA6 matrix. By changing the PP–MA2 by a more functionalized PP–MA containing 8 wt% of reactive maleic anhydride groups (PP–MA8), the phase morphology exhibits a significant change. The particle size of the dispersed phase is much smaller than that of the blend modified with PP–MA2 (compare Fig. 9(b) and (b′)). The superiority of compatibilization efficiency induced by PP–MA8 over PP–MA1 has been demonstrated previously in a binary blend of PP with polycyclohexylmethacrylate (PCHMA) containing amine functionalized PS–NH2 [50]. Fig. 9(b′) shows that the encapsulation of PP particles by PS phase is partial (see circles particles). Indeed, small particles of polystyrene are located at the interface between the PP particles and the PA6 matrix.

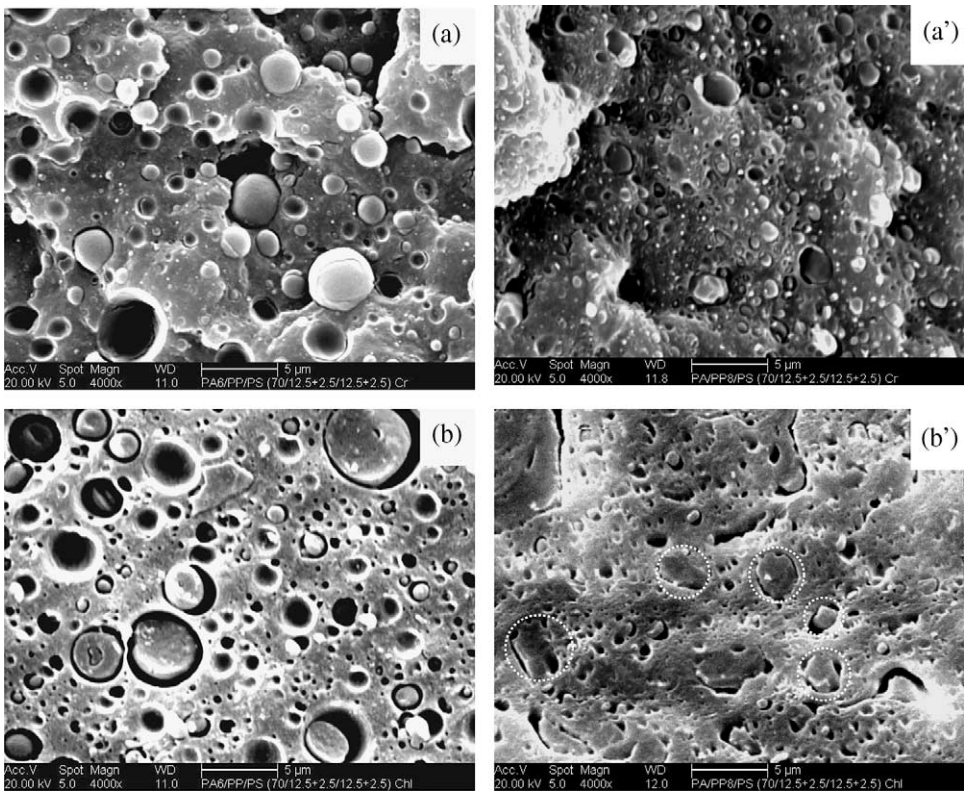


Fig. 9. Morphology of the 70PA6/(12.5/2.5)(PP/PP–MA2)/(12.5/2.5)(PS/SMA2) (a, b) and 70PA6/(12.5/2.5)(PP/PP–MA8)/(12.5/2.5)(PS/SMA2) (a′, b′) blends: (a, a′) cryofractured, (b, b′) cryosmoothed surfaces.

No visible and neat PS shells are visible around the PP core. The effect of the reactive compatibilization on the encapsulation process is very clear. The reduction of the interfacial tension between PA6 matrix and the PP or the PS phase could cause separation between the PS and the PP particles. The balance of interaction between the various immiscible pairs is modified with respect to the uncompatibilized blends favoring the PS phase to distribute separately in the PA6 matrix.

The in situ formed PS-*g*-PA6 copolymer resulting from the grafting reaction between the polyamide molecules and the styrene-*co*-maleic anhydride SMA2 stabilizes the PS particles in the PA6 matrix.

### *3.2.2. 40PA6/30PP/30PS blends*

In Fig. 10 are presented the SEM micrographs of uncompatibilized 40PA6/30PP/30PS blends. The cryo-fracture surfaces (Fig. 10(a)) show a complex phase morphology where it is not possible to identify which phase is located where. In Fig. 10(b) is shown a SEM micrograph of a cryosmoothed surface of the same blend from which the polystyrene phase was extracted using chloroform selective solvent. This solvent treatment revealed that the PS phase constitutes a continuous phase as indicated by the hollow continuous space in between the other two phases. A few percentage of the PS phase is also dispersed in the other phases. This picture does not allow to indicate 'which phase is which' and where the sub-inclusions of the PS phase are located? The chloroform-extracted sample has been further treated with formic acid, a selective solvent for the PA6 phase. Unfortunately, the remaining PP based structure was not self-supporting and collapsed surfaces were obtained that does not allow to characterize the state of the phases. The SEM picture of Fig. 10(c) is obtained from a sample where only PA6 was selectively extracted. It reveals that the PA6 is in the form of droplets on the observed surface. Does the PA6 phase form a dispersion or is it continuous? The quantitative extraction experiments carried out on the same blends using formic acid confirmed that PA6 is continuous (Table 4). Indeed, almost all the PA6 phase was extracted from the blend by the formic acid solvent (97%). That means that the PA6 phase is certainly elongated in a network structure in the extrusion direction as we have demonstrated recently in other blend system [50]. It is thus clear that the three blend components form a three phase-*co*-continuous morphology. Furthermore, a close observation of the extraction data in Table 4 reveals that in the blends of 40PA6/30PP/30PS about 3 wt% of polyamide are dispersed as sub-inclusions in the PP phase.

Upon the substitution of 5 wt% of PP and 5 wt% of PS by their respective compatibilizer precursors, i.e. PP–MA2 or PP–MA8, and SMA2, respectively, the phase morphology has been modified deeply. To identify which of the phases is where in the blend, a compatibilized blend of 40PA6/(25/5)(PP/PP–MA2)/(25/5)(PS/SMA2) is analyzed by SEM (Fig. 11). The cryofractured surfaces observed (Fig. 11(a)) do not allow to identify the phases. In Fig. 11(b) is shown a SEM picture of the cryosmoothed surfaces of the same blends after extraction of the PS phase. As it is seen, the remaining two phases, polyamide and polypropylene, seem composed of a very dense

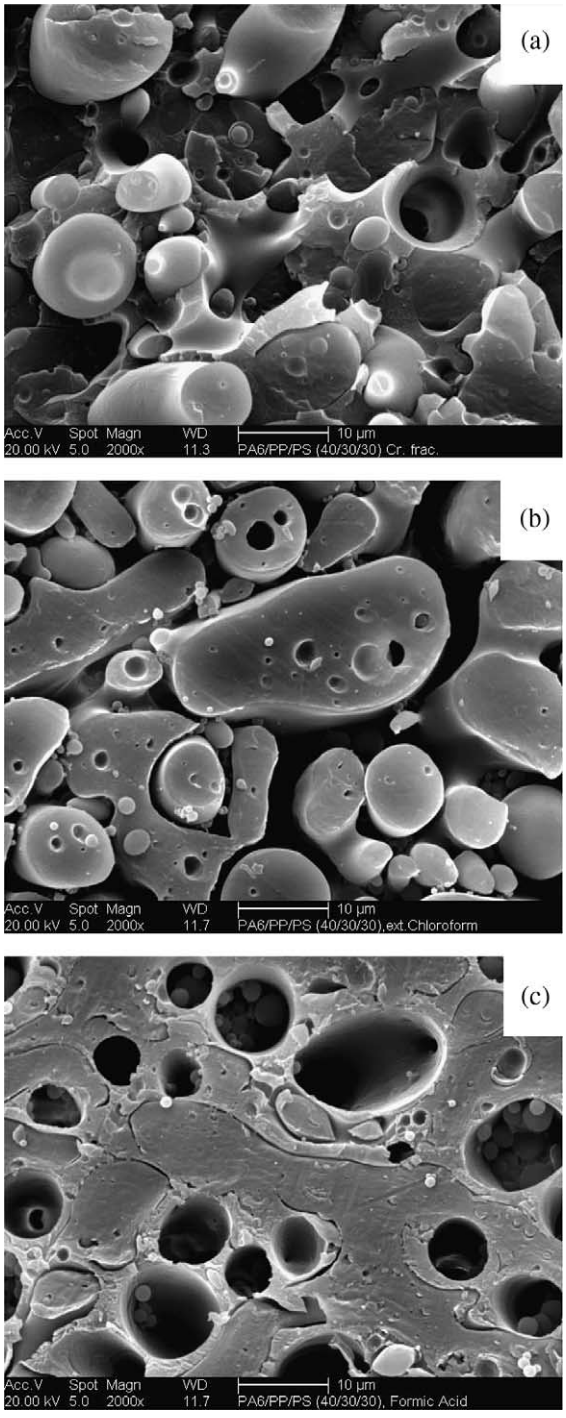


Fig. 10. Morphology of the 40PA6/30PP/30PS blend: (a) cryofractured, (b) chloroform extracted, (c) formic acid extracted surfaces.

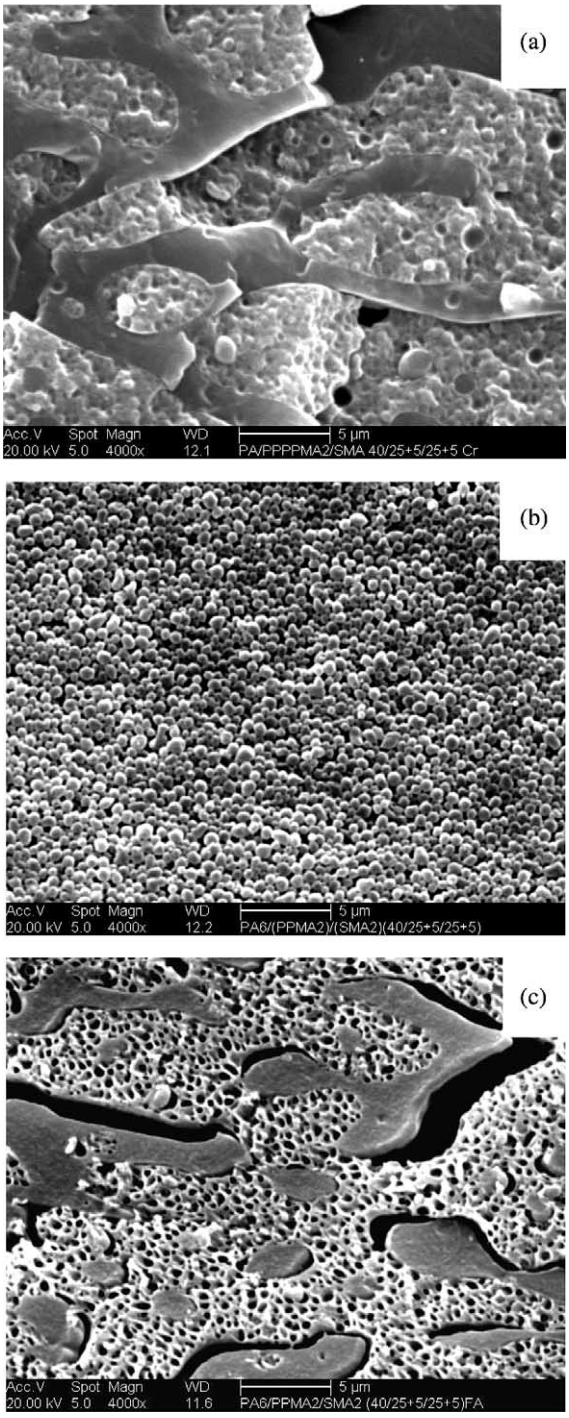


Fig. 11. Morphology of the 40PA6/(25/5)(PP/PP–MA2)/(25/5)(PS/SMA2) blend: (a) cryofractured, (b) chloroform extracted, (c) formic acid extracted surfaces.

Table 4
Co-continuity index of 40PA6/30PP/30PS blend

| Component | Co-continuity index |
|---|---|
| PA6 | 96.9 |
| PS | 100.6 |
| PP | 103.7 |

and interconnected granular particles. Were these particles precipitated as a layer after the removal of polystyrene phase or do they constitute the bulk of polyamide or polypropylene remaining phases? To address this question a further selective extraction of phase is necessary. In Fig. 11(c) is illustrated a SEM micrograph of the same blend where PA6 phase has been removed using formic acid. The observed picture reveals very useful information on the state of polyamide phase. Indeed, as

indicated by the hollow black space on the picture, the polyamide phase is mainly dispersed in PS phase and also forms a layer in between PS an PP phases.

When the compatibilizer precursor for the PA6/PP polymer pairs PP–MA2 is replaced by PP–MA8, containing 4 times higher amount of maleic anhydride, the phase morphology situation of the ternary blends is completely different.

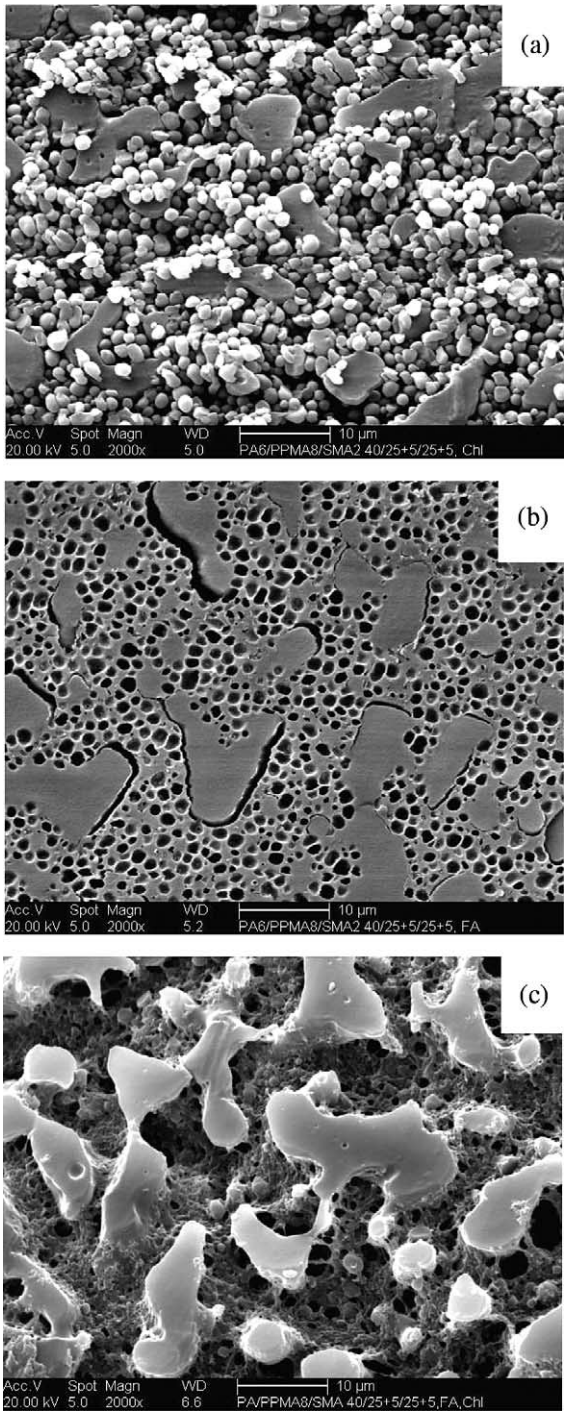


Fig. 12. Morphology of the 40PA6/(25/5)(PP/PP–MA8)/(25/5)(PS/SMA2) blend: (a) cryosmoothed and chloroform extracted, (b) formic acid extracted, (c) PA6 phase extracted with formic acid after PS phase extraction with chloroform.

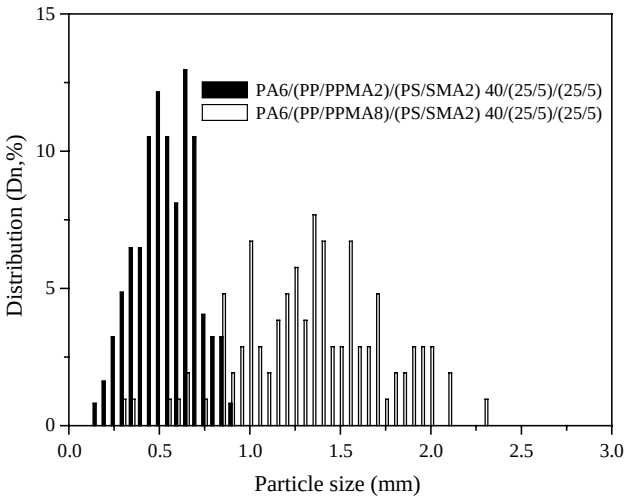


Fig. 13. PA6 dispersed particles size distribution of 40PA6/(25/5)(PP/PP–MA)/(25/5)(PS/SMA2) ternary compatibilized blends, in the presence of PP–MA2 and PP–MA8 compatibilizer precursors.

In Fig. 12(a) is shown the SEM picture of the same blends of 40PA6/(25/5)(PP/PP–MA8)/(25/5)(PS/SMA2) after extraction of the PS phase using chloroform. The two remaining phases are clearly visible but no distinction can be made between the PA6 and the PP phases. The SEM picture of the blend in which the polyamide phase is extracted is shown in Fig. 12(b). It shows that the PA6 phase is included as granules in one of the PP or PS phase and also entrapped in between them as a thin layer.

In order to see where is included the PA6, this phase has been extracted with formic acid from a sample from which PS has already been removed. The SEM picture of that blend shown in Fig. 12(c) reveals indeed that the PA6 is preferably included in the PS phase (note that no holes are left on the PP remaining phase). However, a significant difference lies in the size of the granules of polyamide phase.

Indeed, in the blend of 40PA6/(25/5)(PP/PP–MA2)/(25/5)(PS/SMA2) the PA6 phase have an average particle size of 0.5 μm, whereas in the same composition of 40PA6/(25/5)(PP/PP–MA8)/(25/5)(PS/SMA2) blend the particle size is almost 3 times larger. Fig. 13 reveals that not only the size of the PA6 particles is larger in the case of the blend modified with the combination of (PP–MA8, SMA2), but also their size distribution is broader.

Now, it is clear that in the case of reactively compatibilized PA6/(PP/PP–MA)/(PS/SMA2) ternary blends (having a compatibilization precursor PP–MA2 or PP–MA8) with 40/(25/5)

Table 5
The value of the average particle size for the uncompatibilized PA6/PP/PS and compatibilized PA6/(PP/PP-MA)/(PS/SMA) blends

| Component | Composition | Average particle size of PA6 phase $\bar{D}_n$, (μm) |
|---|---|---|
| PA6/PP/PS | 40/30/30 | Co-continuous |
| PA6/(PP/PPMA2)/(PS/SMA2) | 40/(25/5)/(25/5) | 0.5 |
| PA6/(PP/PPMA8)/(PS/SMA2) | 40/(25/5)/(25/5) | 1.3 |

Table 6
DSC data of pure crystallizable polymers and its binary and ternary blends

| Blends | Composition | PA6 | | PP | |
|---|---|---|---|---|---|
| | | $T_c$ (°C) | $T_m$ (°C) | $T_c$ (°C) | $T_m$ (°C) |
| PA6 | | 189 | 221 | – | – |
| PP | | – | – | 121 | 163 |
| PA6/PP | 70/30 | 188 | 221 | 122 | 163 |
| PA6/PP/PPMA2 | 70/25/5 | 188 | 221 | 122 | 163 |
| PA6/PP/PPMA8 | 70/25/5 | 188 | 221 | 122 | 163 |
| PA6/PS/SMA2 | 70/30/0 | 189 | 221 | – | – |
| | 70/25/5 | 185 | 220 | – | – |
| PA6/PP/PS | 70/15/15 | 187 | 220 | 113 | 161 |
| | 40/30/30 | 187 | 221 | 112 | 159 |
| PA6/(PP/PPMA2)/(PS/SMA2) | 70/(12.5/2.5)/(12.5/2.5) | 186 | 220 | 121 | 163 |
| | 40/(25/5)/(25/5) | 93 | 221 | 110 | 165 |
| PA6/(PP/PPMA8)/(PS/SMA2) | 70/(12.5/2.5)/(12.5/2.5) | 183 | 219 | 121 | 163 |
| | 40/(25/5)/(25/5) | 185; 158; 109 | 217 | 119 | 162 |

/(25/5) composition, PS and PP phases form co-continuous structures with PA6 phase mainly dispersed in PS and also forms a layer in between them. However, substantial differences in PA6 phase size differences exist between the two blend compositions and also between blends modified with PP–MA2 and PP–MA8 precursors.

This opposite effect can only be explained if we consider the adverse 'parasite' effect of the presence of the other reactive system (PA6/PS/SMA2). We believe that as the MA content in PP–MA is increased much more interactions with SMA2 have taken place in the blend, restraining and limiting the efficiency and availability of PP–MA8 at the PP/PA6 interface (Table 5).

### 3.3. Crystallization of PA6 and PP in the ternary blends

As it can be seen from Table 6 and Fig. 14, the melting points ($T_m$) and bulk crystallization temperatures ($T_c$) of the PA6 and PP crystallizable homopolymers are 221 and 188 °C for the PA6, and 163 and 122 °C for the PP phase, respectively. These values have not changed in uncompatibilized and compatibilized binary PA6/PP and PA6/PS blends as well as in uncompatibilized ternary PA6/PP/PS blends. It is now well known that the crystallization behavior of a crystallizable polymer dispersed in a matrix depends on the size of its particles. Overviews of crystallization phenomena in a variety of immiscible polymer blends are given by Frensch et al. [51] and Groeninckx et al. [52]. Recently, a more quantitative study has been performed by Pompe et al. [53] on reactively compatibilized PA/PP blends. Authors [54] indicates that the crystallization of a droplets of minor phase dispersed in a matrix can clearly be affected by the type and miscibility of the compatibilizer used. In the 40PA6/(25/5)(PP/PP–MA2)/(25/5)(PS/SMA2) blends having dispersed PA6 particles the average particle size of which is about 0.5 μm, the crystallization exotherm appearing at $T_c = 188$ °C, typical of bulk PA6 has disappeared and a new exotherm appeared at a temperature of 93 °C (Fig. 14(b), and Table 6). This has also been observed by several other authors for reactively

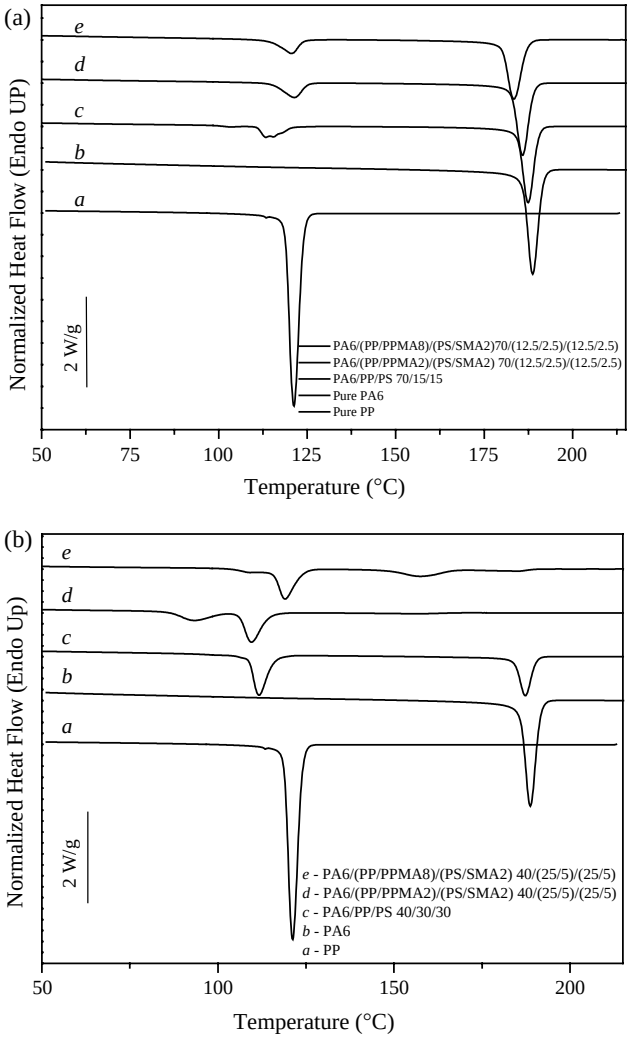


Fig. 14. DSC exotherms of: (a) pure components and uncompatibilized 70PA6/15PP/15PS and compatibilized 70PA6/(12.5/2.5)(PP/PP–MA2)/(12.5/2.55)(PS/SMA2) 70PA6/(12.5/2.5)(PP/PP–MA8)/(12.5/2.55)(PS/SMA2) blends; (b) pure components and uncompatibilized 40PA6/30PP/30PS, compatibilized 40PA6/(25/5)(PP/PP–MA2)/(25/5)(PS/SMA2) and 40PA6/(25/5)(PP/PP–MA8)/(25/5)(PS/SMA2) blends.

compatibilized PMMA/PA6 blends at a temperature within 90–100 °C range and for (PS/SMA2)/PA6 blends at 85 °C [36,55,56].

The following explanation has been proposed for these crystallization phenomena [54]. When the sample is composed of a matrix/droplet phase morphology, heterogeneous nucleation of the crystallizable polymer (PA6 in this case) is restricted to the volume of the droplet. Each droplet will crystallize according to the number and type of heterogeneities present in it. There is a correlation between the phase morphologies and crystallization phenomena of the crystallizable component in a blend. If the particles size distribution of the dispersed component is broad, some fraction of the droplets can be nucleated by the heterogeneities, whereas the droplets that do not contain any heterogeneities (or are smaller enough than the size of a heterogeneity) can undergo homogeneous nucleation at a larger degree of supercooling (in this case at a temperature of 93 °C).

In the 40PA6/(25/5)(PP/PP–MA8)/(25/5)(PS/SMA2) blend compatibilized using the reactive precursors combination, (PP–MA8 + SMA2), the average particle size is larger (1.3 μm) and the size distribution is broader, multiple fractionated crystallization of PA6 phase are observed at the temperatures of 181, 158 and 109 °C (Fig. 14).

## 4. Conclusions

Melt blending of polyamide 6, polystyrene and polypropylene homopolymers form immiscible ternary blend. Depending on the composition either a dispersed encapsulated or not) or a co-continuous three phase morphologies are developed.

Uncompatibilized ternary 70PA6/15PP/15PS blends exhibit an encapsulated phase morphology having polypropylene cores and polystyrene shells in opposition to the prediction of Harkin's spreading coefficient and free interfacial energy concept. This failure was ascribed to the substantial differences in viscosities between the dispersed components. The addition of the two compatibilizing reactive system, i.e. maleic anhydride grafted polypropylene and styrene-*co*-maleic anhydride changed partly the situation but still encapsulated structures were observed.

In the ternary blends having almost equal amount of PA6, PP and PS (i.e. composition of 40PA/30PP/30PS) a three-phase co-continuous morphology was developed. Their reactive compatibilization using the reactive precursors mentioned above caused the PA6 phase to get dispersed preferentially in the polystyrene phase. The differences in PA6 particle size observed by scanning electron microscopy were confirmed by the crystallization behavior where the crystallization due to heterogeneous nucleation has completely disappeared and new crystallization exotherms resulting from homogeneous nucleation have emerged.

## Acknowledgements


- Research Fund KULeuven (GOA Project 98/06).
- Fund for Scientific Research-Flanders, Belgium.
- T. S. Omonov gratefully acknowledges the Research Council of the Catholic University of Leuven for providing a research scholarship (August 2002 – December 2004).
- Prof P. Moldenaers for the use of equipment (Rheological measurement).


## References


[1] Scobbo JJ. Macromol Chem Macromol Sympos 1992;57:345–52.
[2] Hachiya H, Takayma S, Takeda K. J Appl Polym Sci 1998;70(12): 2515–20.
[3] Molina MJ, Morales E, Lamantina FP. Polym Networks Blends 1995; 5(3):141–5.
[4] Moussaif N, Jerome R. Polymer 1999;40(14):3919–32.
[5] Vivier T, Xanthos M. J Appl Polym Sci 1994;54(5):569–75.
[6] Xanthos M, Patel A, Dey S, Dagli SS, Jacob C, Nosker TJ, et al. Adv Polym Technol 1994;13(3):231–9.
[7] Xanthos M, Grenci J, Patel SH, Patel A, Jacob C, Dey S, et al. Polym Compos 1995;16(3):204–14.
[8] Numata S, Fujii Y. Plast Rubber Compos Process Appl 1995;24(5): 293–300.
[9] Ha CS, Park HD, Cho WJ. J Appl Polym Sci 1999;74(6):1531–8.
[10] Tall S, Albertsson AC, Karlsson S. J Appl Polym Sci 1998;70(12): 2381–90.
[11] Krulis Z, Kokta BV, Horak Z, Minkova D, Fortenly I. Macromol Mater Eng 2001;286(3):156–60.
[12] Ha CS, Park HD, Cho WJ. J Appl Polym Sci 2000;76(7):1048–53.
[13] Fang ZP, Zeng MF, Cai GP, Xu CW. J Appl Polym Sci 2001;82(12): 2947–52.
[14] Reignier J, Favis BD, Heuzey M-C. Polymer 2003;44(1):49–59.
[15] Campbell JR, Hobbs SY, Shea TJ, Watkins VH. Polym Eng Sci 1990; 30(17):1056–62.
[16] Favis BD, Therrien D. Polymer 1991;32(8):1474–81.
[17] Hobbs SY, Dekkers ME, Watkins VH. Polymer 1988;29(9):1598–602.
[18] Guo HF, Packirisamy S, Gvozdic NV, Meier DJ. Polymer 1997;38(4): 785–94.
[19] Guo HF, Gvozdic NV, Meier DJ. Polymer 1997;38(19):4915–23.
[20] Harkin WD. The physical chemistry of surface films. New York: Reinhold; 1952.
[21] Dedecker K, Groeninckx G. Polymer 1998;39(21):4985–92.
[22] Wu S. Polym Eng Sci 1987;27:335.
[23] Wu S. Polymer 1985;26(12):1855–63.
[24] Oshinski AJ, Keskkula H, Paul DR. Polymer 1992;33(2):268–83.
[25] Oshinski AJ, Keskkula H, Paul DR. Polymer 1992;33(2):284–93.
[26] Fayt R, Jerome R, Teyssie R. ACS Sym Ser 1989;395:38.
[27] Cimmino S, Coppola F, D'Orazio L, Greco R, Maglio G, Malinconinco M, et al. Polymer 1986;27(12):1874–84.
[28] González-Montiel A, Keskkula H, Paul DR. Polymer 1995;36(24): 4587–603.
[29] Dedecker K, Groeninckx G. Polymer 1998;39(21):5001–10.
[30] Sundararaj U, Macosko CW. Macromolecules 1995;28(8):2647–57.
[31] Majumdar B, Keskkula H, Paul DR. Polymer 1994;35(7):1386–98.
[32] Galloway JA, Koester KJ, Paasch BJ, Macosko CW. Polymer 2004;45: 423–8.
[33] Wu S. Polym Eng Sci 1987;27:335.
[34] Macosko CW. Rheology, principles, measurements, and applications. Weinheim: VCH Publishers; 1994 [chapter 4].
[35] Fried JR, Hanna GA. Polym Eng Sci 1982;22:705.
[36] Dedecker K, Groeninckx G. Polymer 1998;39(21):4993–5000.
[37] Wu S. Polymer interface and adhesion. New York: Marcel Dekker; 1982 [chapter 3].
[38] Wilkinson AN, Clemens ML, Harding VM. Polymer 2004;45: 5239–49.
[39] Chandavasu C, Xanthos M, Sirkar KK, Gogos CG. Polymer 2002;43(3): 781–95.

[40] Kirjava J, Rundqvist T, Holsti-Miettinen R, Heino M, Vainio T. J Appl Polym Sci 1995;55(7):1069–79.
[41] Chappelear DC. ACS Polym Prepr 1964;5:363.
[42] Son Y. Polymer 2001;42(3):1287–91.
[43] Elemans PHM, Janssen JMH, Meijer HEH. J Rheol 1990;34(8): 1311–25.
[44] Cho K, Jeon HK, Park CE. Polymer 1996;37(7):1117–22.
[45] Verdier C, Vinagre HTM, Piau M, Joseph DD. Polymer 2000;41(17): 6683–9.
[46] Jannerfeldt G, Boogh L, Mañson J-AE. J Polym Sci, Part B: Polym Phys 1999;37(16):2069–77.
[47] Asthana H, Jayaraman K. Macromolecules 1999;32(10):3412–9.
[48] Arashiro EY, Macaùbas PHP, Demarquette NR. Anais do 4° Congresso Brasileiro de Polìmeros (ABPol), Brasil 1997 p. 530.
[49] Macaùbas PHP, Demarquette NR. Polymer 2001;42(6):2543–54.
[50] Harrats C, Omonov TS, Groeninckx G, Moldenaers P. Polymer 2004; 45(24):8115–26.
[51] Frensch H, Harnischfeger P, Jungnickel BJ. In: Utracki LA, Weiss RA, editors. Multiphase polymers: blends and ionomers. ACS symposium series, vol. 395; 1989, 1989. p. 101.
[52] Groeninckx G, Vanneste M, Everaert V. In: Utracki LA, editor. Polymer blends handbook. Crystallization, morphological structure and melting of polymer blends, vol. 1. Dordrecht: Kluwer Academic Publishers; 2002. p. 203–94 [chapter 3].
[53] Pompe G, Potschke P, Pionteck J. J Appl Polym Sci 2002;86(13):3445–53.
[54] Ikkala OT, Holstimiettinen RM, Seppälä J. J Appl Polym Sci 1993;34: 3234.
[55] Tol RT, Mathot VBF, Groeninckx G. Polymer 2005;46:2955–65.
[56] Tol RT, Mathot VBF, Reynaers H, Goderis B, Groeninckx G. Polymer 2005;46.